J. Nonlinear Funct. Anal. 2022 (2022) 30 https://doi.org/10.23952/jnfa.2022.30

MATHRES Journal of Nonlinear Functional Analysis
Available online at http://jnfa.mathres.org

AN $L1$ IMAGE DECOMPOSITION METHOD BASED ON FRAMELET ANALYSIS PRIOR WITH ANISOTROPIC TOTAL VARIATION

HUASONG CHEN[1], QIANSHENG FENG[1,*], HAO QIANG[2], YUANYUAN FAN[1], TINGYU SHENG[3]

[1]Faculty of Mathematics and Physics, Huaiyin Institute of Technology, Huaian 223001, China
[2]Faculty of Computer and Software Engineering, Huaiyin Institute of Technology, Huaian 223001, China
[3]Academy of Medical Engineering and Translational Medicine, Tianjin University, Tianjin 300072, China

Abstract. Image decomposition is an important and challenging problem in image processing. This paper proposes an $L1$ cartoon-texture image decomposition method. To separate the cartoon, we use framelet analysis prior to regularize cartoon, and employ an anisotropic total variation to enhance the edges of the separated images while eliminate the annoying stair-casing often emerging in total variation based methods. In order to remove the high frequency part (such as noise and texture) in cartoon, a simple quadratic term is added in cartoon separation. The texture is then separated by using a common discrete cosine transform. Also, an $L1$ fidelity term is proposed to estimate the least absolute deviation between the ground truth and the measured images. An alternating Bregman algorithm is developed to solve the double-variable and multi-$L1$ minimization problem. The experiments show that the proposed method provides better image decomposition than other methods.

Keywords. Anisotropic total variation; Framelet analysis prior; Image decomposition; $L1$ fidelity; multi-variable optimization.

1. INTRODUCTION

Image decomposition is an interesting and important task in image processing. The main goal of image decomposition is to separate an image into a cartoon structure and texture component. Cartoon represents the geometric structure with homogeneous regions (such as, edges, and flat region). Texture models the oscillating part with small scales. Now, image decomposition methods have been successfully applied to a broad range of areas including biomedical or medical imaging, remote imaging, astronomical sensing, and image restoration [2,8,19–21,24,27].

The first prior based models proposed for image decomposition are based on variational functions [1,3,4,18,29,38], which introduce total variation (TV) operators to extract the strong edge

*Correspoinding author.
E-mail addresses: chenhuasong@hyit.edu.cn (H. Chen), fqs2008@hyit.edu.cn (Q. Feng), qianghaonjust@gmail.com (H. Qiang), fyuanyuan@hyit.edu.cn (Y. Fan), shengtingyu@tju.edu.cn (T. Sheng).

Received August 11, 2021; Accepted June 22, 2022.

structure from an given image, and employ another functions to represent texture. TV-based image decomposition model can be described as:

$$\inf_{(u,v)\in BV\times K/v=u_c+u_t}\Big(\int |Du_c| + \lambda\Phi(u_t)\Big), \tag{1.1}$$

where $\int |Du_c|$ is the total variation (TV) of u_c [34]. The function $\Phi(u_t)$ can be $L2$ norm [17], $L1$ norm [18], G space function [29], and Hilbert space function [38], where the penalty function $\Phi(u_t)$ can be:

$$\Phi(u_t) = \begin{cases} \|u_t\|_{L2}^2, \\ \|u_t\|_G, \\ \|u_t\|_{L1}, \\ \|u_t\|_H^2, \end{cases} \qquad \Phi(u_t) = \|u_t\|_{L2}^2. \tag{1.2}$$

For a more detailed review on variational image decomposition, we refer the reader to [4, 18]. TV based methods have been proved to be efficient on image decomposition. However, these methods often suffered from the well-known stair-casing effect caused by TV, especially on the image edges [33].

In [36, 37], a novel image decomposition method was proposed based on the sparse representation of images, which is usually called Morphological Component Analysis (MCA). MCA assumes that every component of an image can be sparsely represented in a specific transform domain by a dictionary. When one dictionary can efficiently represent one component of image in sparse domain, it would be highly inefficient in representing the other parts of images. The cost function of MCA is:

$$\{\alpha_t^{opt}, \alpha_n^{opt}\} = \arg\min_{\{\alpha_t,\alpha_n\}} \|\alpha_t\|_1 + \|\alpha_t\|_1 + \lambda\|u - T_t\alpha_t - T_n\alpha_n\|_2^2 + \gamma TV\{T_n\alpha_n\} \tag{1.3}$$

where T_t and T_n are the selected dictionaries for texture u_t and u_n cartoon, respectively, and α_t and α_n are the sparse coefficients of texture and cartoon in the transformed domain. The TV regularization is employed for enhancing the edge of cartoon. To recover an image, cartoon $u_n = T_n\alpha_n$, and texture $u_t = T_t\alpha_t$. Recently, Boblin et al. developed multichannel MCA [5] and the generalized MCA [5,6] for a generalized blind signal separation. MCA can efficiently separate an image into several components with individual characteristics, however, it also uses TV to enhance the edges because of the weak ability of sparse representation on edge-preserving. This may introduce the stair-casing effect on the edges. Recently, Minaee and Wang proposed an image segmentation algorithm to decompose the background and foreground by using a sparse-smooth segmentation technique [30, 31]. They used the synthesis operator to model the smooth background with the assumption that the foreground part is sparse. Later, they added a total variation term as a combination regularization term for foreground [32]. The proposed algorithms achieved good performance on segmenting the foreground and the background. However, it is a little bit different with the work cartoon-texture decomposition which implements the decomposition task under the consideration that different component of images has different scales with different properties.

Decomposing an image into cartoon and texture automatically is a nontrivial work. Neither TV-based methods nor MCA discuss how to more efficiently extract cartoon or texture from an image without other components. This is because the computer often mistakes some texture

as structure when details contain sufficiently strong contrast. In order to overcome the drawbacks of TV used in image decomposition task [1, 3, 4, 7, 18, 29, 32, 38], this paper proposes an image decomposition model, which is based on framelet based analysis prior, anisotropic total variation (ATV). We employ framelet analysis prior to separate the cartoon from images, and use anisotropic total variation model to enhance the edges. Also in order to remove the texture details mistaken as cartoon, we introduce a quadratic term for cartoon cost function. Moreover, we proposed a $L1$ norm to replace the traditional $L2$ norm fidelity functional to improve the decomposition performance. The main contributions of this paper:

(1) A novel image decomposition model based on framelet analysis prior with ATV is proposed.

(2) A $L1$ norm fidelity term for robust image decomposition us proposed.

(3) An alternating Bregman iteration optimization algorithm is proposed to solve the proposed multi-variable and multi $L1$ optimization problem.

(4) Extensive experiments are conducted on images with various characteristics. Detailed objective and subjective comparisons with existing state-of-the-art methods are presented.

The rest parts of this paper are organized as follows: Brief review of sparse representation and anisotropic total variation and the proposed model are represented in Section 2. Numerical algorithm based a modified Bregman iteration is described in Section 3. Experimental are shown in Section 4. And conclusions are given in Section 5, the last section.

2. Related work and proposed model

Before introducing our proposed model, we begin with the brief review of the framelet system and anisotropic total variation.

2.1. **Framelet system.**

Framelet system is the wavelet tight frame, which needs no down-sampling. This paper will chose the popular piece wise linear B-spline framelet system, which is simple and easy to implement for our experiments. If

$$g = \sum_{p \in D} \langle g, p \rangle p, \quad \forall g \in L_2(R), \tag{2.1}$$

then we call $D \in L_2(R)$ as a tight frame of $L_2(R)$. $\langle g, p \rangle$ is the inner product of two functions g and p.

A tight frame is often constructed by a collection of dilations and shifts of a scaling function with a refinement mask as:

$$D(P) := \{p_{i,j,1} : 1 \le i \le r; j, l \in Z\} \quad with \quad p_{i,j,1} := 2^{j/2} p_i(2^j . - l), \tag{2.2}$$

where $D(P)$ is the tight wavelet frame, and $p_i, i = 1, 2, \ldots, r$ are the framelets. In the discrete setting, suppose that a vector denote an image, and the framelet transform operator D is a matrix. Then the coefficient vector created by framelet system can be represented as:

$$\alpha = Df \tag{2.3}$$

Then the image can be simply reconstructed by an inverse operator D^T

$$f = D^T \alpha. \tag{2.4}$$

We emphasize that D is a matrix whose row dimension is larger than its column dimension. Also, D is often called the analysis operator, and D^T is the synthesis operator. Both analysis

operator and synthesis operator have been successfully applied into many image processing tasks, which present different properties. In general, $D^T D = I$ with $D^T D \neq I$. This means that the framelet system is redundant and non-orthogonal wavelet system. For more detailed analysis, we refer to the readers to [9, 22].

2.2. **Anisotropic total variation.** The edge is an important feature of images. Numerous methods that consider image decomposition have applied edge-preserving models, such as, total variation (TV), Framelet, Curvelet etc. TV is an efficient and most used one. This is due to its strong edge-preserving capability. However, TV often suffers from the undesired stair-casing on the edges, which contain some rectangular structure, such as, corners. In [26], an anisotropic total variation (ATV) was proposed to eliminate the stair-casing. The definition of ATV can be described as the following penalty term

$$\int_\Omega \varphi(\bigtriangledown u) := \sup_{g \in C_c^1(\Omega;R^n), g(x) \in W_\varphi} \int_\Omega u(x) divg(x) dx, \quad \forall x \in \Omega, \tag{2.5}$$

where $\varphi : R^n \to R$ is a convex, and one-homogeneous function with the origin at 0, and the set of W_φ is defined as:

$$W_\varphi := \{y \in R^n : x \cdot y \leq \varphi(x), \quad \forall x \in R^n\}. \tag{2.6}$$

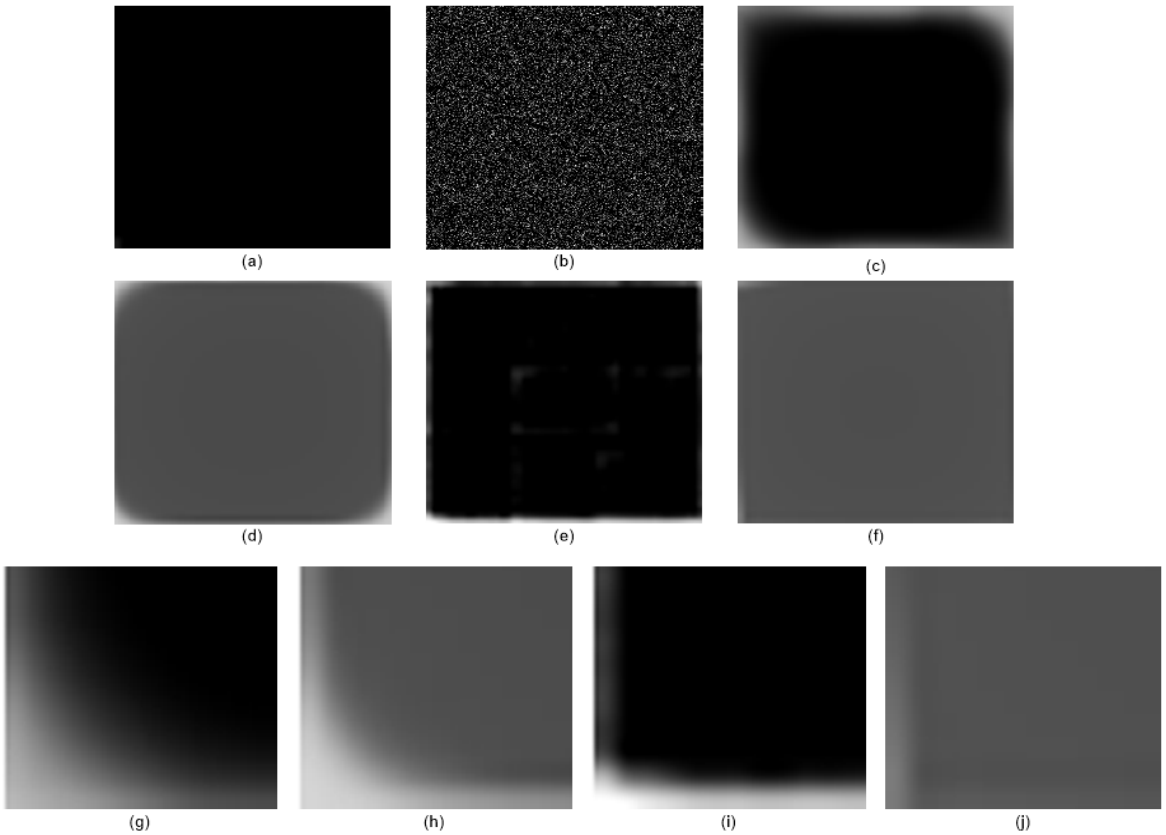

FIGURE 1. Comparison of edge-preserving properties. (a) Original rectangular image; (b) noisy image; (c) TV restoration[14]; (d) TV-Bregman restoration; (e) sparse presentation restoration [10]; (f) ATV restoration [26]: The last row: the zoomed lower-left corners of (c), (d), (e), (f).

The set is the closed unit square Wulff shape, which is compatible with anisotropy of function φ with $\varphi(x,y) = |x| + |y|$. ATV has the better ability to protect the sharp edges of images. Figure 1 shows the edge-preserving comparison of the ATV and other popular methods. The results in Figure 1 show that ATV outperforms on edge-preserving than other methods, especially on the corners of edges.

2.3. **The proposed model.** Due to the multi-level decomposition properties of sparse representation in some sparse domains. MCA is a useful and popular model for image decomposition. For an image f to be decomposed into cartoon $_u$ and texture v with corresponding sparse coefficient α_u and T_v transformed by operator α_u and T_v, MCA can be described as:

$$\min_{u,v} L(f, T_u^T \alpha_u, T_n^T \alpha_n) + \Phi(\alpha_u) + \Psi(\alpha_u) + TV(T_u^T \alpha_u), \tag{2.7}$$

where the fidelity term is designed as the Euclidean distance between f and $T_u^T \alpha_u + T_n^T \alpha_n$. Cartoon and texture terms are regularized by $L1$ norm of the α_u and α_n. The edges of cartoon are enhanced by the well-known TV regularization. MCA uses the synthesized representations, which explore the most sparse solution among all transform coefficients which often brings visible artifacts along image edges (see Figure 1.(e) for details). Also, due to the stair-casing effect, TV in the model of (2.7) often introduces the notorious stair-casing which often distort the edge texture, such as, corners (see Figure 1.(c) and (d) for details).

Inspired by recently works on analysis-based sparse representation [10] and the ATV [26], we propose an image decomposition model by using analysis-based sparse representation and anisotropic total variation. Analysis-based sparse representation tends to have better visual results than the synthesis-based approach [10,11]. And ATV is superior to preserving and enhancing edges than TV and sparse representation as shown in Figure 1. The proposed decomposition model is:

$$\begin{aligned} \{u_c, u_t\} = \arg\min_{u_c,u_t} & |u_c + u_t - f|_1 + \alpha_1 \|D_c u_c\|_1 + \beta_1 \|u_c\|_2^2 \\ & + \alpha_2 \|D_t u_t\|_1 + \beta_2 (\|\nabla_x u_c\|_1 + \|\nabla_y u_c\|_1), \end{aligned} \tag{2.8}$$

where $\alpha_1, \alpha_2, \beta_1$ and β_2 are the positive regularization parameters, D_c and D_t are two analysis sparse transform operators, and u_c and u_t are the cartoon and texture of image f to be decomposed. The requirement $f = u_c + u_t$ says that the decomposition part u_c and u_c should be approximate to the original image. The term $\|D_c u_c\|_1$ is to extract the cartoon from image, and the quadratic term $\beta_1 \|u_c\|_2^2$ is to filter the high frequency part in cartoon (such as noise and texture). The combination of analysis regularization and quadratic term has been proved that it would lead to more stable results than that of the non-quadratic term [12, 13, 16]. In other words, the combination of $\|D_c u_c\|_1 + \|u_c\|_2^2$ would extract more better cartoon results without or with more less texture structure than non-quadratic term. This may generate more satisfactory separation results. Term $\|D_t u_t\|_1$ is to separate the texture part, and the last two terms are the anisotropic total variation of cartoon to enhance the edges of cartoon. The elements of $\nabla_x u_c$ and $\nabla_y u_c$ are given by:

$$\nabla_x u_{c(i,j)} = u_{c(i+1,j)} - u_{c(i,j)} \quad \textit{and} \quad \nabla_y u_{c(i,j)} = u_{c(i,j+1)} - u_{c(i,j)}, \tag{2.9}$$

where (i, j) is the pixel coordinate of image.

Remark 2.1. The model of (2.8) is similar to but different from the work of MCA which uses synthesis based sparse representation. First, this paper uses analysis-based representation,

which leads to different results. Synthesis based approach tends to seek for the most sparse solution among the coefficients. Hence, only a small number of atoms are applied to describe the image signal. Each atom plays an important role in signal representation. However, any additional errors in atoms would lead to the solution far away from the desired description [25]. On the other hand, the atoms in analysis representation have the equivalent choice to describe the image signal and minimize the dependence on each individual one, which would lead to the stable solution in the recovery process [8, 10, 19, 20]. Also we employ the ATV instead of TV to enhance the edges, which can eliminate the annoying stair-casing effect arisen in MCA. Moreover, we propose to employ the $L1$ cost function for fidelity term. $L1$ cost function has been proved to generate the better geometrical features than common $L2$ function [15, 18, 23].

Remark 2.2. The quadratic term is applied to smooth the oscillating component existing in the cartoon. Another $L2$ regularization of gradient β_2 is often used for smoothing. As well studied, $L2$ gradient term often over-regularizes the edges and corners, which cause the final edges blurring [16]. This is because that the noise in the edges would be amplified after gradient transformation, which causes the edge gradients to be more noisy. To remove the noise, it must smooth the edge gradient with larger weights, which cause the final results over-smoothing. Instead, quadratic term avoids the over-smoothing. Moreover, the quadratic term combined with the sparse gradient or the sparse coefficients can protect the edges with more robust edge structure [13, 16]. In addition, $\min_{u_c} \|D_c u_c\|_1 + \beta_1 \|u_c\|_2^2$ can converge to $\min_{u_c} \|D_c u_c\|_1$ as $\beta_1 \to 0$. This was analyzed and proved in details in [12, 13].

3. Numerical algorithm

For $L1$ and multi-variable minimization problems with model (2.8), there is no existing method, which can directly solve this complex optimization problem. Fortunately, we found that multi-variable optimization problem can be decomposed into several single-variable sub-problems by using alternative algorithm(AM) [14]. Then the $L1$ norm optimization problem can be efficiently solved by using some iterative methods, such as, alternating direction method (ADM) [40], proximal gradient method [35], split Bregman iteration [28] etc. The methods are equivalent to each other under some conditions. For more review and discussion of optimization methods, we refer to reader to [39]. In this paper, we apply the AM into the Bregman iteration method to solve the multi-variable and multi-$L1$ optimization problem in model (2.8).

Due to the multi-variable optimization, model (2.8) can be transformed into following two subproblem groups by using AM [13]:

$$\begin{aligned} u_c^{k+1} = &\arg\min_{u_c} |(u_c + u_t^k) - f|_1 + \alpha_1 \|D_c u_c\|_1 + \beta_1 \|u_c\|_2^2 \\ &+ \beta_2 (\|\nabla_x u_c\|_1 + \|\nabla_y u_c\|_1), \end{aligned} \tag{3.1}$$

and

$$u_t^{k+1} = \arg\min_{u_t} |(u_c + u_t^k) - f|_1 + \alpha_2 \|D_t u_t\|_1, \tag{3.2}$$

Step 1: For u_c^{k+1}, introduce auxiliary variables d_0, d_1, p_1, p_2 and let

$$d_0 = u_c + u_t - f, d_1 = D_c u_c, p_1 = \nabla_x u_c, p_2 = \nabla_y u_c. \tag{3.3}$$

Then problem (3.1) can be transformed into following optimization problem by using Split Bregman methods [35]:

$$
\begin{aligned}
(u_c^{k+1}, d_0^{k+1}, d_1^{k+1}, p_1^{k+1}, p_2^{k+1}) = \underset{u_c, d_1, p_1, p_2}{\arg\min} \; & |d_0|_1 + \frac{\lambda_0}{2}\|d_0 - u_c + u_t - f\|_2^2 \\
& + \alpha_1 \|d_1\|_1 + \frac{\lambda_1}{2}\|d_1 - D_c u_c - b_1^k\|_2^2 \\
& + \beta_2 \|p_1\|_1 + \frac{\lambda_3}{2}\|p_1 - \nabla_x u_c - q_1^k\|_2^2 \\
& + \beta_2 \|p_2\|_1 + \frac{\lambda_4}{2}\|p_2 - \nabla_y u_c - q_2^k\|_2^2,
\end{aligned} \tag{3.4}
$$

and

$$
\begin{cases}
b_1^{k+1} = b_1^k + D_c u_c^{k+1} - d_1^{k+1}, \\
q_1^{k+1} = q_1^k + \nabla_x u_c^{k+1} - p_1^{k+1}, \\
q_2^{k+1} = q_2^k + \nabla_y u_c^{k+1} - p_2^{k+1}, \\
b_0^{k+1} = b_0^k + u_c^{k+1} + u_t^{k+1} - f - d_0^{k+1}.
\end{cases} \tag{3.5}
$$

Using alternating algorithm again, problem (3.4) can be separated into

$$
\begin{aligned}
u_c^{k+1} = \arg\min_{u_c} \; & \frac{\lambda_0}{2}\|d_0^k - (u_c + u_t^k - f) - b_0^k\|_2^2 + \frac{\lambda_1}{2}\|d_1^k - D_c u_c - b_1^k\|_2^2 \\
& + \beta_1 \|u_c\|_2^2 + \frac{\lambda_3}{2}\|p_1^k - \nabla_x u_c - q_1^k\|_2^2 + \frac{\lambda_4}{2}\|p_2^k - \nabla_y u_c - q_2^k\|_2^2,
\end{aligned} \tag{3.6}
$$

and

$$
\begin{cases}
d_1^{k+1} = \arg\min_{d_1} \alpha_1 \|d_1\|_1 + \frac{\lambda_1}{2}\|d_1 - D_c u_c^{k+1} - b_1^k\|_2^2, \\
p_1^{k+1} = \arg\min_{p_1} \beta_2 \|p_1\|_1 + \frac{\lambda_3}{2}\|p_1 - \nabla_x u_c^{k+1} - q_1^k\|_2^2, \\
p_2^{k+1} = \arg\min_{p_2} \beta_2 \|p_2\|_1 + \frac{\lambda_4}{2}\|p_2 - \nabla_y u_c^{k+1} - q_2^k\|_2^2, \\
d_0^{k+1} = \arg\min_{d_0} \|d_0\|_1 + + \frac{\lambda_0}{2}\|d_0^k - (u_c + u_t^k - f) - b_0^k\|_2^2.
\end{cases} \tag{3.7}
$$

Using the direct differentiation, the linear function of u_c subproblem in (3.6) is:

$$
\begin{aligned}
(\lambda_1 D_c^T D_c + 2(\beta_1 + \lambda_0) I + \lambda_3 \nabla_x^T \nabla_x + \lambda_4 \nabla_y^T \nabla_y) u_c^{k+1} = \lambda_0 (d_o^k + f - u_t^k - b_o^k) + \\
\lambda_1 D_c^T (d_1^k - b_1^k) + \lambda_3 \nabla_x^T (p_1^k - q_1^k) + \lambda_4 \nabla_y^T (p_2^k - q_2^k).
\end{aligned} \tag{3.8}
$$

Then FFT can be employed to obtain the final iteration formula of problem (3.8) as done in [6, 19, 20]. Problem (3.7) are the standard soft shrinkage as analyzed in [35], and the iterative solutions of (3.5)-(3.6) can be given as:

$$d_0^{k+1} = shrink(u_c^{k+1} + u_t^k - f + b_0^k, \frac{1}{\lambda_0}) \tag{3.9}$$

and

$$d_1^{k+1} = shrink(D_c u_c^{k+1} + b_1^k, \frac{\alpha_1}{\lambda_1}); \tag{3.10}$$

$$p_1^{k+1} = shrink(\nabla_x u_c^{k+1} + q_1^k, \frac{\beta_2}{\lambda_3}) \tag{3.11}$$

and

$$p_2^{k+1} = shrink(\nabla_y u_c^{k+1} + q_2^k, \frac{\beta_2}{\lambda_4}), \tag{3.12}$$

where $shrink(x, \chi) = \frac{x}{|x|} \cdot max(|x| - \chi, 0)$

Step 2: For u_2^{k+1}, introduce an auxiliary variable d_2 , and let $d_2 = D_t u_t$. Then problem (3.2) can be transformed as:

$$\begin{cases} (u_t^{k+1}, d_2^{k+1}) = \arg\min\limits_{u_t, d_2} \alpha_2 |d_2|_1 + \dfrac{\lambda_0}{2} \|d_0 - (u_c^{k+1} + u_t - f) - b_0^{k+1}\|_2^2 \\ \qquad\qquad + \dfrac{\lambda_2}{2} \|d_2 - D_t u_t - b_2^k\|_2^2 \\ b_2^{k+1} = b_2^k + D_t u_t^{k+1} - d_2^{k+1}. \end{cases} \tag{3.13}$$

Using alternating algorithm, problem (3.13) can be separated into

$$u_t^{k+1} = \arg\min_{u_t} \frac{\lambda_0}{2} \|d_0 - (u_c^{k+1} + u_t - f) - b_0^{k+1}\|_2^2 + \frac{\lambda_2}{2} \|d_2^k - D_t u_t - b_2^k\|_2^2, \tag{3.14}$$

and

$$d_2^{k+1} = \arg\min_{d_2} \alpha_2 \|d_2\|_1 + \frac{\lambda_2}{2} \|d_2 - D_t u_t^{k+1} - b_2^k\|_2^2. \tag{3.15}$$

The linear function of in (3.14) is

$$(\lambda_0 I + \lambda_2 D_t^T D_t) u_t^{k+1} = d_0^{k+1} + f - u_c^{k+1} - b_0^{k+1} + \lambda_2 D_2^T (d_2^k - b_2^k). \tag{3.16}$$

Using FFT method can obtain the corresponding algorithm. The solution of (3.15) is

$$d_2^{k+1} = shrink(D_t u_t^{k+1} + b_2^k, \frac{\alpha_2}{\lambda_2}). \tag{3.17}$$

Based on the above formulas, the iteration algorithm of the proposed algorithm can be given in Algorithm 1.

*Algorithm*1

1.*Initialize* : $u_c^0 = u_t^0 = 0, d_1^0 = b_1^0 = 0, d_2^0 = b_2^0 = 0, p_1^0 = q_1^0 = 0, p_2^0 = q_2^0$.

2.*For* $k = 1,2,\ldots,$ *or* $\|u^{k+1} - u^k\|_2 / \|u^{k+1}\|_2 > tol$, *repeat* :

Step 1:fixing u_t^k, d_2^k, b_2^k, update:

u_c by formula (3.8)

$$d_1^{k+1} = shrink(D_c u_c^{k+1} + b_1^k, \alpha_1/\lambda_1),\ b_1^{k+1} = b_1^k + D_c u_c^{k+1} - d_1^{k+1},$$

$$p_1^{k+1} = shrink(\nabla_x u_c^{k+1} + q_1^k, \beta_2/\lambda_3),\ q_1^{k+1} = q_1^k + \nabla_x u_c^{k+1} - p_1^{k+1},$$

$$p_2^{k+1} = shrink(\nabla_y u_c^{k+1} + q_2^k, \beta_2/\lambda_4),\ q_2^{k+1} = q_2^k + \nabla_y u_c^{k+1} - p_2^{k+1},$$

$$d_0^{k+1} = shrink(u_c^{k+1} + u_t^k - f + b_0^k, 1/\lambda_0),\ b_0^{k+1} = b_0^k + u_c^{k+1} + u_t^{k+1} - f - d_0^{k+1}.$$

Step 2:fixing $u_c^{k+1}, d_1^{k+1}, b_1^{k+1}, p_1^{k+1}, p_2^{k+1}, q_1^{k+1}, q_2^{k+1}$, update:

u_t by formula (3.14)

$$d_2^{k+1} = shrink(D_t u_t^{k+1} + b_2^k, \alpha_2/\lambda_2),\ b_2^{k+1} = b_2^k + D_t u_t^{k+1} - d_2^{k+1}.$$

3.*Output* $u_c^{k+1} + u_t^{k+1}$

4. Experiments

4.1. **Image decomposition parameter tuning.** This subsection mainly discusses the parameter selection and shows the decomposition results of the proposed decomposition algorithm. The stopping criterion is $\|u^{k+1} - u^k\|_2 / \|u^{k+1}\|_2$, and the iteration stopping values are set as $tol = 5 \times 10^{-6}$ for decomposition. All the tests were conducted under MATLAB 2011. In our experiments, four test images are " Barbara", "Bitplane","Circuit Board" with the size of 512×512 as shown in Figure 2. The analysis operator for cartoon regularization is the framelet [9] as described in Section 2.1, and the operator for texture representation is discrete cosine transform (DCT) as used in [19, 20].

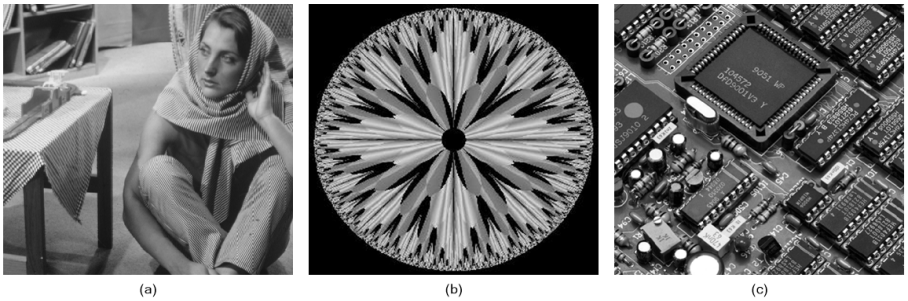

(a) (b) (c)

FIGURE 2. Test images with different contents. (a) Barbara, (b) Bitplane image, (c) Circuit Broad.

First, we show the convergence curves of the Algorithm 4 in Figure 3. The curves show that Algorithm 4 converges after several iterations on all test images. However, iterations for different images are different due to the differences of the image content. The more the content information is, the more iterations the image needs.

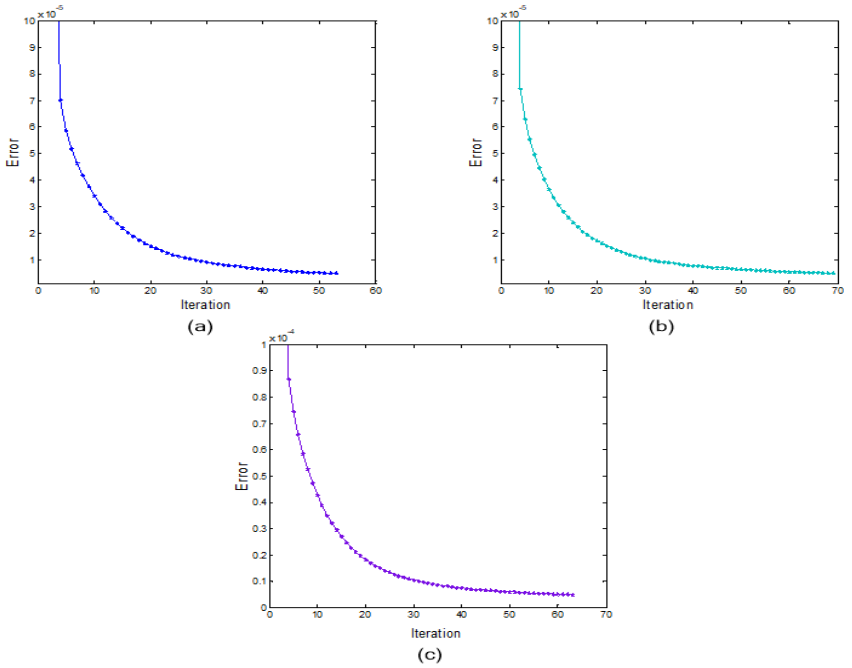

FIGURE 3. The iteration curves of the proposed method. (a) Babara, (b) Bit-plane, (c) Circuit Broad.

Then, we report the decomposition results with varying parameters $\alpha_1, \alpha_2, \beta_1$ and β_2. The test results are shown in Figure 4, and the corresponding zoomed results are shown in Figure 5. It is found that the rate of α_1/α_2 has an important impact on the decomposition results. When the $\alpha_1/\alpha_2 > 1$, the cartoon part contains much texture which is undesired (shown as Figure 4.(b) and Figure 4.(b)), and the smaller the value of α_1/α_2. When $\alpha_1/\alpha_2 < 1$, the decomposition result becomes better (shown as Figure 4.(a) and Figure 5.(a)). The values of β_1 and β_2 also play an important role on image decomposition. Figure 4.(c)-(d) and Figure 5.(c)-(d) show the comparison with different values of β_1. It is found that the bigger the values of β_1, the worse the decomposition is. The cartoon often suffers from the over-smoothing effect with large β_1. The same phenomenon occurs on parameter β_2 (as shown in Figure 4.(e)-(f) and Figure 5.(e)-(f)). After several tests, we find that the decomposition results are good when: $\alpha_1/\alpha_2 \in [0.01, 0.2]$, $\alpha_1 \in [8\times10^{-4}, 8\times10^{-2}]$, $\beta_1 \in [0, 10^{-5}]$ and $\beta_2 \in [10^{-5}, 0.5]$.

This paper sets $\alpha_1/\alpha_2 = 0.1$, $\alpha_1 = 6\times10^{-2}$, $\beta_1 = 0.95\times10^{-9}$, and $\beta_2 = 0.08$ for all decomposition tests, and the bregman iteration parameters are set as: $\lambda_0 = 0.05$, $\lambda_1 = 2\times10^{-2}$, $\lambda_2 = 8\times10^{-2}$, and $\lambda_3 = \lambda_4 = 4\times10^{-2}$.

FIGURE 4. The analysis of decomposition results for different parameter values of $\alpha_1, \alpha_2, \beta_1$ and β_2; (a) $\alpha_1 = \alpha_2 = 8 \times 10^{-2}$, (b) $\alpha_1/\alpha_2 = 10$, (c) $\beta_1 = 10^{-3}$, (d) $\beta_1 = 10^{-6}$, (e) $\beta_2 = 5 \times 10^{-4}$, (f) $\beta_2 = 1$

.

FIGURE 5. The analysis of decomposition results for different parameter values of $\alpha_1, \alpha_2, \beta_1$ and β_2; (a) $\alpha_1 = \alpha_2 = 8 \times 10^{-2}$, (b) $\alpha_1/\alpha_2 = 10$, (c) $\beta_1 = 10^{-3}$, (d) $\beta_1 = 10^{-6}$, (e) $\beta_2 = 5 \times 10^{-4}$, (f) $\beta_2 = 1$

.

4.2. **Image decomposition results and comparison.** To show the performance of the proposed decomposition algorithm, we show the decomposition results on image "Bitplane" and "Barbara", and also we have the comparison with several state-of-art decomposition methods which are: TV-G space method [29], TV+L1 decomposition method [18], Fast decomposition filters [3], directional filters [4], and MCA decomposition method [27, 36].

The comparison results are shown in Figure 6 and Figure 8. For a further visual comparison, the zoomed regions of results in Figure 6 and Figure 8 are presented in Figure 7 and Figure 9, respectively. It is shown that all the methods can decompose an image well, and our decomposition results are comparable to those of other methods. Furthermore, our method performs with better vision effect (see Figure 6.(f)-Figure 9.(f)). Cartoon results of TV+G space method and MCA method still have a little visual texture (see Figure 7.(a),(e) and Figure 9.(a),(e)). On contrary, thecartoon results of TV+L1 method lose some visual structure and texture results contain some part, which is suitable in cartoon (see Figure 7.(b) and Figure 9.(b)). Texture results of fast filters and directional filters have relatively poor visual texture structure (see Figure 7 and Figure 9.(c)-(d)) . Instead, the decomposition results of our method have good vision effect.

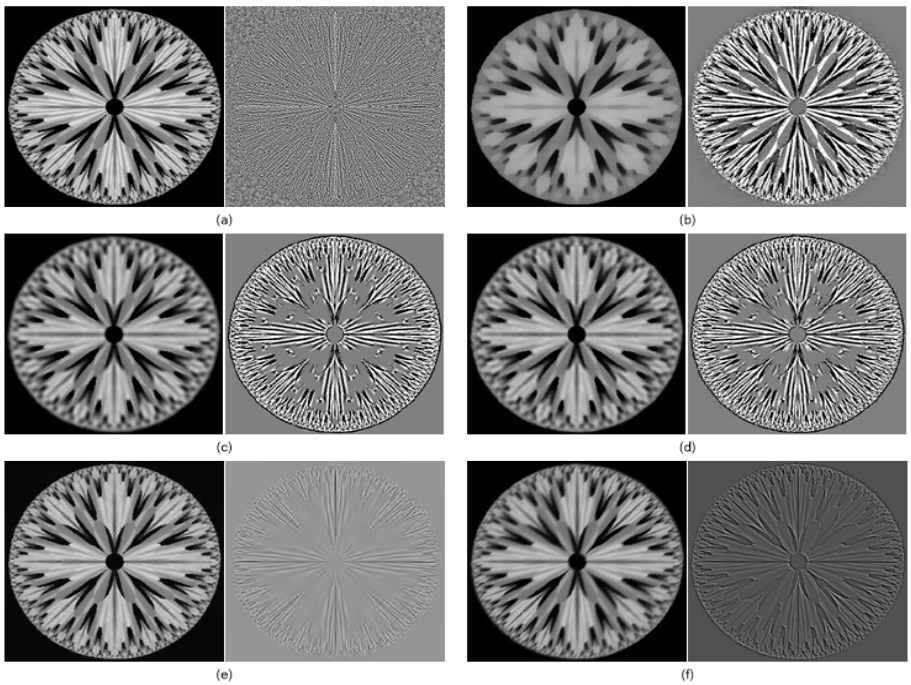

FIGURE 6. The comparison of decomposition results on image "Bitplane"; (a) TV+G, (b) TV+L1, (c) Fast decomposition filters, (d) directional filters, (e) MCA, (f) the proposed decomposition method.

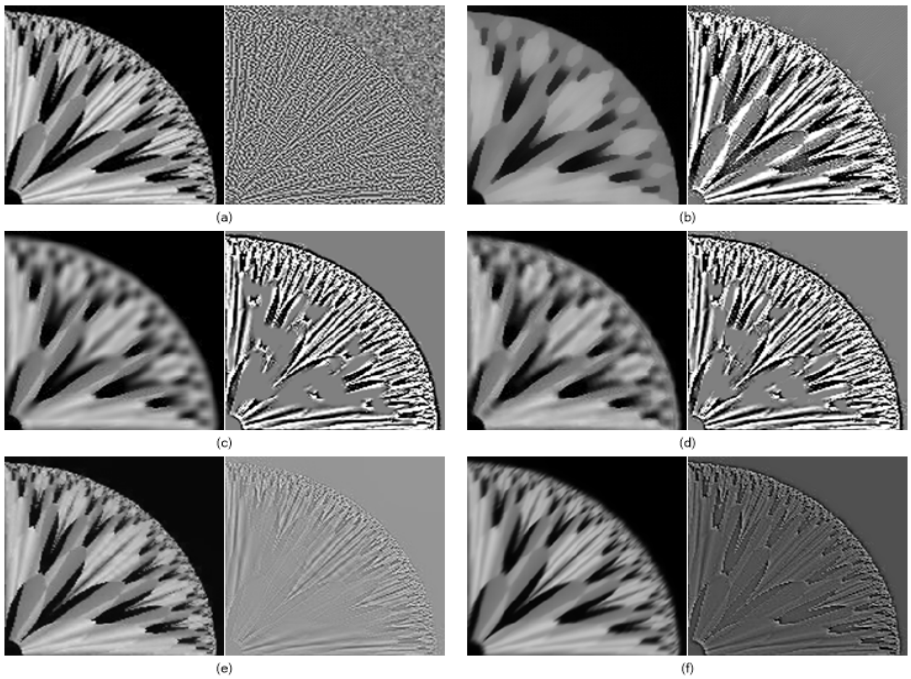

FIGURE 7. The zoomed region comparison of decomposition results on image "Bitplane"; (a) TV+G, (b) TV+L1, (c) Fast decomposition filters, (d) directional filters, (e) MCA, (f) the proposed decomposition method.

FIGURE 8. The comparison of decomposition results on image "Barbara"; (a) TV+G, (b) TV+L1, (c) Fast decomposition filters, (d) directional filters, (e) MCA, (f) the proposed decomposition method.

FIGURE 9. The zoomed region comparison of decomposition results on image "Barbara"; (a) TV+G, (b) TV+L1, (c) Fast decomposition filters, (d) directional filters, (e) MCA, (f) the proposed decomposition method.

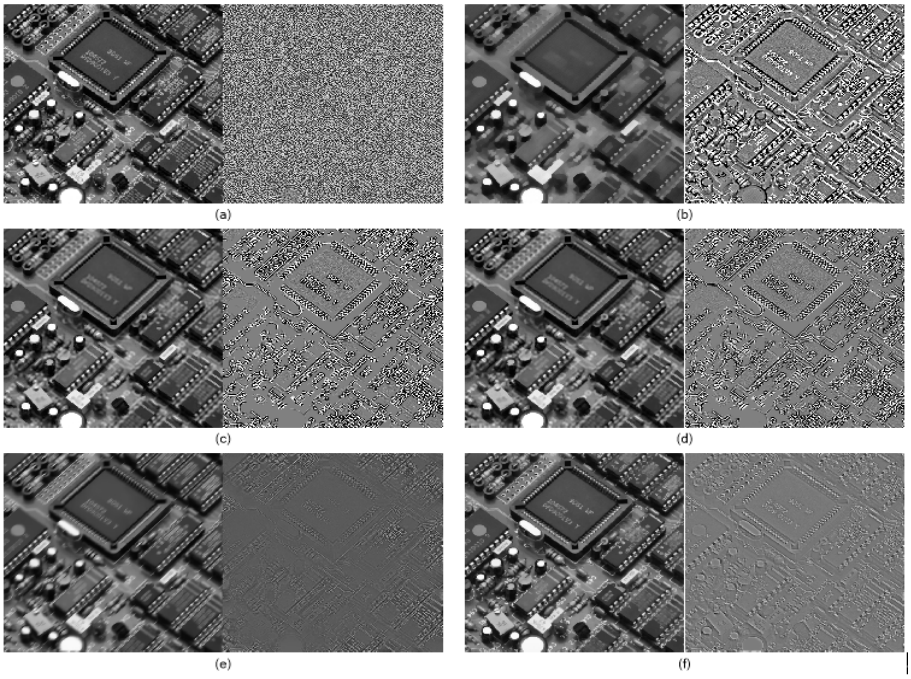

FIGURE 10. The comparison of decomposition results on image "Circuit Broad"; (a) TV+G, (b) TV+L1, (c) Fast decomposition filters, (d) directional filters, (e) MCA, (f) the proposed decomposition method.

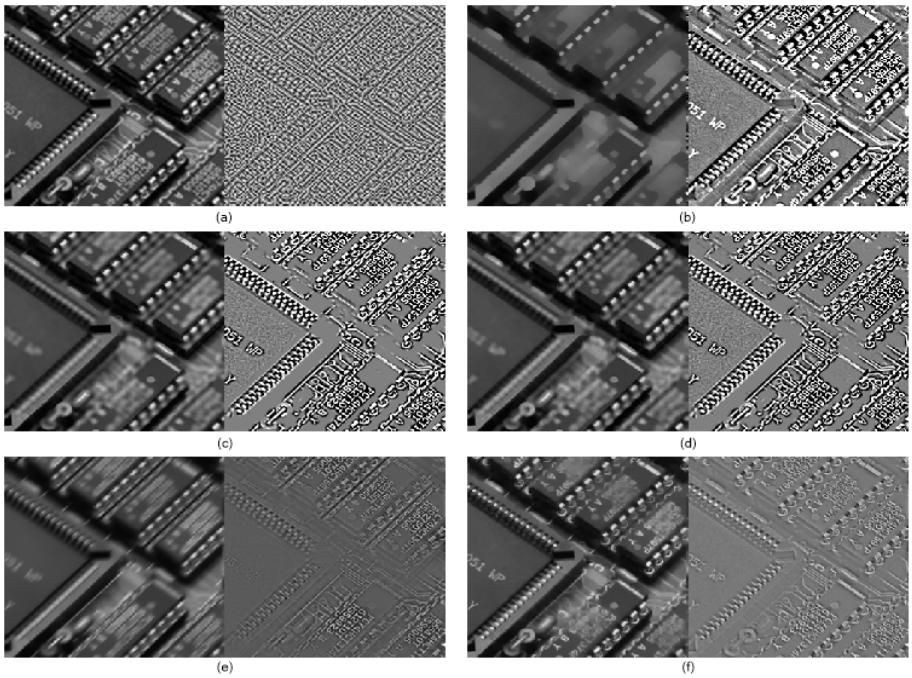

FIGURE 11. The zoomed region comparison of decomposition results on image "Barbara"; (a) TV+G, (b) TV+L1, (c) Fast decomposition filters, (d) directional filters, (e) MCA, (f) the proposed decomposition method.

5. CONCLUSION

This paper proposed an $L1$ fidelity based image decomposition model by using framelet based analysis spare representation and anisotropic total variation with a quadratic term. Then a multi-variable Bregman iteration algorithm was developed to solve the proposed method. Numerical experiments showed that the proposed method has a better performance than those of recent state-of-art methods on image decomposition. However, this paper still exists a disadvantage that the sparse operators are preselected, the decomposition results are based on the selection of the operators. How to design the adaptive sparse operators for image decomposition and its applications in image processing is main aim of our further work.

REFERENCES

[1] J.F. Aujol, G. Gilboa, T. Chan, S. Osher, Structure-texture image decomposition—modeling, algorithms and parameter selection, Int. J. Comput. Vision 67 (2006) 111-136.

[2] M. Bertalmio, L. Vese, G. Sapiro, S. Osher, Simultaneous structure and texture image inpainting, IEEE Trans. Image Process. 12 (2003) 882-889.

[3] A. Buades, T.M. Le, J.M. Morel, L.A. Vese, Fast cartoon plus texture image filters, IEEE Trans. Image Process. 19 (2010) 1978-1986.

[4] A. Buades, J.L. Lisani, Directional filters for color cartoon plus texture image and video decomposition, J. Math. Imaging Vis. 55 (2016) 125-135.

[5] J. Boblin, J.L. Starck, J. Fadili, Y. Moudden, Sparsity and morphological diversity in blind source separation, IEEE Trans. Image Process. 16 (2007) 2662-2674.

[6] J. Boblin, J.L. Starck, Y. Moudden, M.J. Fadili, Blind source separation: the sparsity revolution, Adv. Imaging Electron Phys. 152 (2008) 221-306.

[7] J. Boblin, Y. Moudden, J. Fadili, J.L. Starck, Morphological diversity and sparsity for multichannel data restoration, J. Math. Imaging Vis. 33 (2009) 149-168.
[8] J. Cai, R.H. Chan, Z. Shen, Simultaneous cartoon and texture inpainting, Inverse Probl. Imaging 4 (2010) 379-395.
[9] J. Cai, B. Dong, Z. Shen, Image restoration: A wavelet frame based model for piecewise smooth functions and beyond, Appl. Comput. Harmon. Anal. 41 (2016) 94-138.
[10] J. Cai, B. Dong, Z. Shen, Image restorations: A wavelet frame based model for piecewise smooth functions and beyond, Appl. Comput. Harmon. Anal. 41 (2016) 94-138.
[11] J. Cai, S. Osher, Z. Shen, Split Bregman method and frame based image restoration, SIAM Multiscale Modeling and Simulation, 8 (2009) 337-369.
[12] J. Cai, S. Osher, Z. Shen, Linearized Bregman Iterations for compressed sensing, Math. Comput. 78 (2009) 1515-1536.
[13] J. Cai, H. Ji, C. Liu, Z. Shen, Blind motion deblurring from a single image using sparse approximation, 2009 IEEE Conference on Computer Vision and Pattern Recognition, pp. 104-111, 2009.
[14] T. Chan, C. Wong, Convergence of the alternating minimization algorithm for blind deconvolution, Linear Algebra Appl. 316 (2000) 259-285.
[15] T.F. Chan, S. Esedo, Aspects of total variation regularized $L1$ function approximation, SIAM J. Appl. Math. 65 (2005) 1817-1837.
[16] G. Chavenet, K. Kunisch, Regularization of linear least squares problems by total bounded variation, ESAIM: Control, Optim. Cal. Var. 2 (1997) 359-376.
[17] A. Chambolle, P.L. Lions, Image recovery via total variation minimization and related problems, Numer. Math. 76 (1997), 167-188.
[18] T.F. Chan, S. Esedoglu, Aspects of total variation regularized $L1$ function approximation, SIAM J. Appl. Math. 65 (2005) 1817-1837.
[19] H. Chen, X. Qu, Y. Jin, Z. Li, A. He, A cartoon-texture decomposition based image deblurring model by using framelet based sparse representation, Proc. SPIE 1002012 (2016) 1-13. doi: 10.1117/12.2245929.
[20] H. Chen, Q. Wang, C. Wang, et al, Image decomposition based blind image deconvolution model by employing sparse representation, Iet Image Process. 10 (2016) 908-925.
[21] H. Chen, J. Liu, Q. Feng, Y. Fan, A structure decomposition based method for restoring images corrupted by impulse noise, Proc. SPIE 10817 (2018). 10.1117/12.2500592.
[22] I. Daubechies, B. Han, A. Ron, Z. Shen, Framelets: MRA-based constructions of wavelet frames, Appl. Comput. Harmon. Anal. 14 (2003) 1-46.
[23] V. Duval, J.F. Aujol, Y. Gousseau, The Tv l1 model: A geometric point of view, Multiscale Model Simul. 8 (2009) 154-189.
[24] M. Elad, J.L. Starck, P. Querre, D.L. Donoho, Simultaneous cartoon and texture image inpainting using morphological component analysis (MCA), Appl. Comput. Harmon Anal. 19 (2005) 340-358.
[25] M. Elad, P. Milanfar, R. Rubinstein, Analysis versus synthesis in signal priors, Inverse Probl. 23 (2007) 947-968.
[26] S. Esedo, S.J. Osher, Decomposition of images by the anisotropic Rudin-Osher-Fatemi model, Commun. Pure Appl. Math. 57 (2004) 1609-1626.
[27] M.J. Fadili, J.L. Starck, J. Bobin, Y. Moudden, Image decomposition and separation using sparse representations: an overview, Proceedings of the IEEE, 98 (2010) 983-994.
[28] T. Goldstein, S. Osher, The split Bregman method for $L1$ regularized problems, SIAM J. Imaging Sci. 2 (2009) 323-343.
[29] Y. Meyer, Oscillating patterns in linage processing and nonlinear evolution equations, vol. 22, University Lecture Series, 2001.
[30] S. Minaee, Y. Wang, Screen content image segmentation using least absolute deviation fitting, IEEE Int. Conference on Image Process. 2015.
[31] S. Minaee, Y. Wang, Screen content image segmentation using robust regression and sparse decomposition, IEEE J. Em. Sel. Top C, 99 (2016) 1-12.
[32] S. Minaee, Y. Wang, Screen content image segmentation using sparse decomposition and total variation minimization, Int. Conference on Image Processing, IEEE, 2016.

[33] M. Nikolova, Local strong homogeneity of a regularized estimator, SIAM J. Appl. Math. 61 (2000) 633-658.
[34] L. Rudin, S. Osher, E.Fatemi, Nonlinear total variation based noise removal algorithms, Physica D, 60 (1992) 259-268.
[35] W. Shi, Q. Ling, G. Wu, et al, A proximal gradient algorithm for decentralized composite optimization, IEEE Trans. Signal Process. 63 (2015) 6013-6023.
[36] J.L. Starck, M. Elad, D. Donoho, Image decomposition via the combination of sparse representatntions and variational approach, IEEE Trans. Image Process. 14 (2005) 1570-1582.
[37] J.L. Starck, M. Elad, D. Donoho, Redundant multiscale transforms and their application for morphological component analysis, In Advances in Imaging and Electron Physics, P. Hawkes, (Ed.), Vol. 132, Academic Press, Elsevier, 2004.
[38] L.A. Vese, S.J. Osher, Modeling textures with total variation minimization and oscillating patterns in image processing, J. Sci. Comput. 19 (2003) 553-572.
[39] C.L. Wu, X.C. Tai, Augmented Lagrangian method, dual methods and split Bregman iteration for ROF, vectoria TV and high order models, SIAM J. Imaging Sci. 3 (2010) 300-339.
[40] J.F. Yang, Y. Zhang, Alternating direction algorithms for $L1$ problems in compressive sensing, SIAM J. Sci. Comput. 33 (2011) 250-278.